

Direct Measurement of Acoustic Spectral Density and Fractional Topological Charge

Hao Ge^{1,§}, Zi-Wei Long^{1,§}, Xiang-Yuan Xu¹, Jin-Guo Hua¹, Yang Liu^{2,3}, Bi-Ye Xie⁴, Jian-Hua Jiang^{2,3,*}, Ming-Hui Lu^{1,5,†} and Yan-Feng Chen^{1,5,‡}


¹*National Laboratory of Solid State Microstructures & Department of Materials Science and Engineering, Nanjing University, Nanjing, Jiangsu 210093, China*

²*Institute of Theoretical and Applied Physics, School of Physical Science and Technology, & Collaborative Innovation Center of Suzhou Nano Science and Technology, Soochow University, 1 Shizi Street, Suzhou, 215006, China*

³*Key Laboratory of Advanced Optical Manufacturing Technologies of Jiangsu Province & Key Laboratory of Modern Optical Technologies of Ministry of Education, Soochow University, Suzhou 215006, China*

⁴*School of Science and Engineering, The Chinese University of Hong Kong, Shenzhen, 518172, China*

⁵*Jiangsu Key Laboratory of Artificial Functional Materials, Nanjing University, Nanjing, Jiangsu 210093, China*

 (Received 9 August 2022; revised 6 December 2022; accepted 23 February 2023; published 22 March 2023)

LDOS is a fundamental spectral property that plays a central role in various physical phenomena, such as wave-matter interactions and spontaneous emissions. The role of LDOS in acoustics was uncovered only in recent years and the measurement of acoustic LDOS has not yet been achieved. Here, we report on the direct measurement of the LDOS in acoustic systems. The acoustic LDOS is quantified here through the measurement of the volume flow rate and the acoustic pressure with a local excitation-probe configuration. Based on this method, we detect the LDOS in the one-dimensional acoustic Su-Schrieffer-Heeger model and observe the fractional topological charge of the system. Our work unveils the role of the LDOS in acoustic phenomena and paves the way toward characterizing and tailoring the LDOS in acoustic systems, which holds promise for applications in acoustic emission control, energy localization, and wave-matter interaction.

DOI: [10.1103/PhysRevApplied.19.034073](https://doi.org/10.1103/PhysRevApplied.19.034073)

I. INTRODUCTION

The bulk density of states (DOS) gives the spectral distribution of the eigenstates of a system, which, in a condensed-matter context, is closely related to the optical, thermal, and transport properties of the underlying material. In quantum electrodynamics, the Purcell effect reveals the LDOS as one of the central quantities that determines the spontaneous emission rate of a quantum emitter [1–5]. The engineering of LDOS by nanophotonic structures is a persistent theme in optics [6–10]. The photonic crystals [5], hyperbolic metamaterials [6,8–10], and plasmonic structures [7] are utilized to tailor light-matter interactions and modify the spontaneous emission rate of emitters. The usefulness of LDOS in acoustics and its relevance to many acoustic phenomena were uncovered only in recent years. The emission of a sound source can

be enhanced by employing acoustic resonant metamaterial structures [11–14], and it was found that the emission enhancement results from the increased LDOS of acoustic systems [15]. The acoustic analog of Drexhage’s experiment was demonstrated [16], where the modification of emission efficiency can be described as the variation of the LDOS caused by the reflective wall. The elastic Purcell effect has also been reported [17], and it shows theoretically that the nanoparticle resonators can suppress or enhance the emission rates of sources by engineering the local density of elastic states. The LDOS plays a key role in various acoustic phenomena, and therefore the measurement of LDOS is helpful for the spatial and spectral control of acoustic emissions. The measurement of LDOS can also serve as a useful tool for the characterization of acoustic systems. However, the direct measurement of LDOS in acoustic systems has not yet been achieved.

In electronic systems, the LDOS at the Fermi level can be probed by the STM using tunneling current [18]. The optical LDOS can be mapped by measuring the fluorescence lifetime of nanoscale emitters [19]. For microwave metamaterials, the LDOS is obtained by inserting a subwavelength antenna into the structure, and measuring

*joejhjiang@hotmail.com

†luminghui@nju.edu.cn

‡yfchen@nju.edu.cn

§These authors contributed equally to this work.

the radiation resistance of the antenna using a microwave network analyzer [20–22]. The radiation resistance of the antenna is proportional to the photonic LDOS. To quantify the photonic LDOS, a reference system with a known LDOS is also needed [21]. In acoustic systems, the LDOS is related to the emission rate of subwavelength monopole sources. The measurement of acoustic LDOS has not yet been achieved, mainly due to the technical challenges in characterizing the acoustic properties of subwavelength monopole sources.

The measurement of LDOS can also help identify the band topology of topological phases. In recent years, topological phases with unprecedented properties have attracted much attention. A rich variety of topological phases have also been realized in acoustic systems, which leads to robust designs and functionalities for acoustic devices. One of the most significant features of topological phases is the bulk-boundary correspondence, which links the existence of in-gap boundary states to the bulk topological invariants. However, for topological crystalline insulators without additional local symmetries, the boundary states may reside within the bulk bands and the bulk-boundary correspondence fails to identify the band topology. Instead, the fractional spectral charge at edge boundaries or disclinations is the key topological feature in these phases [20–22]. The spectral charge can be obtained by integrating the LDOS over the frequency range of an entire bulk band. Recently, it was proposed that the multidimensional partition of LDOS can directly identify topological phases and provide a general correspondence between bulk topology and measurable LDOS [23]. The measurement of LDOS can also contribute to characterize the fragile topology in acoustic metamaterials, where it has a spectral consequence in the form of spectral flow in acoustic systems [24]. The spectral flow and mode localization has also been experimentally demonstrated in elastic media [25], which holds promise for applications in energy localization and elastic wave control.

In this work, we develop a method to directly measure the acoustic LDOS via the integration of a thermal convection-based acoustic particle velocity sensor and a MEMS pressure microphone. Theoretically, the acoustic LDOS is related to the imaginary part of the onsite acoustic Green's function. From the acoustic wave equations, the LDOS can be extracted from the frequency and spatial dependence of the volume flow rate and the acoustic pressure when the acoustic waves are excited by a subwavelength source. The volume flow rate represents the strength of the acoustic source and here is obtained by the acoustic particle velocity sensor. The proposed method can directly acquire the acoustic LDOS without need for a reference system. We demonstrate the underlying principle by measuring the acoustic LDOS of two prototypes of resonators: the Helmholtz resonator and Fabry-Perot resonator. Furthermore, we show that acoustic LDOS can

be used to directly extract the fractional topological charge in the SSH model when it is realized in acoustic metamaterials, revealing a fundamental phenomenon in topological acoustics, which would benefit the study of the fractional charge and localized states at bulk defects in topological phases [26–30]. Our work would open up an avenue to characterize and tailor the LDOS in acoustic systems, and may find applications in acoustic emission control and high-intensity acoustic devices.

II. GREEN'S FUNCTION AND ACOUSTIC LDOS

The acoustic LDOS is related to the imaginary part of the onsite Green's function as follows [31]:

$$\rho(\omega, \mathbf{r}) = \mp \frac{1}{\pi} \frac{dk_0^2(\omega)}{d\omega} \text{Im}G^\pm(\omega, \mathbf{r} = \mathbf{r}'), \quad (1)$$

where \mathbf{r}' and \mathbf{r} denote the positions of the source and the detector, respectively, G^\pm is the retarded and advanced Green's function, and $k_0^2 = \omega^2/c_0^2$ (c_0 is the speed of sound). Assuming the Sommerfeld radiation boundary condition, the retarded Green's function is the solution to the acoustic wave equation with a monopole source of unit strength:

$$\nabla^2 G^+(\omega, \mathbf{r}, \mathbf{r}') + k_0^2 G^+(\omega, \mathbf{r}, \mathbf{r}') = \delta(\mathbf{r} - \mathbf{r}'). \quad (2)$$

The corresponding equation for the acoustic pressure p is

$$\nabla^2 p + k_0^2 p = i\omega \rho_{\text{air}} u_s S_s \delta(\mathbf{r} - \mathbf{r}'), \quad (3)$$

where ρ_{air} is the mass density of air, u_s is the acoustic particle velocity on the surface of monopole source, and S_s is the surface area of the source. The velocity u_s stands for the oscillating velocity of the air flows, which is a useful quantity in describing acoustic wave dynamics. The product of u_s and S_s is the volume flow rate that represents the strength of the source. By comparing Eqs. (2) and (3), Green's function at the source location can be expressed as

$$G^+(\omega, \mathbf{r} = \mathbf{r}') = \frac{p_s}{i\omega \rho_{\text{air}} u_s S_s}, \quad (4)$$

where p_s denotes the acoustic pressure at the source location. The acoustic LDOS is then obtained as

$$\rho(\omega, \mathbf{r}) = \frac{2}{\pi} \frac{1}{\rho_{\text{air}} c_{\text{air}}^2} \text{Re} \left(\frac{p_s}{u_s S_s} \right). \quad (5)$$

Therefore, the acoustic LDOS at the source location is proportional to the radiation resistance of the sound source.

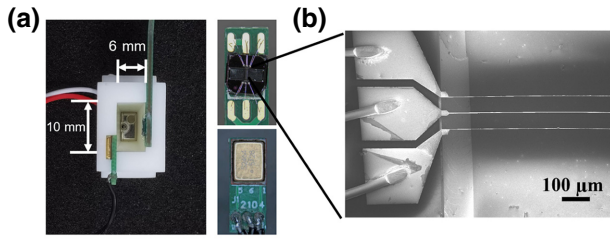


FIG. 1. (a) A compact detector tube, which combines a balanced armature speaker, a homemade acoustic particle velocity sensor, and a Knowles MEMS silicon microphone. The cross-section area of the tube is $10 \times 6 \text{ mm}^2$. (b) Photo of the velocity sensor which consists of three suspended heated wires above a silicon substrate.

III. METHODS FOR MEASURING THE ACOUSTIC LDOS

From Eq. (5), it can be seen that the acoustic LDOS at the source location can be obtained via the acoustic pressure p_s and the volume flow rate of source $u_s S_s$. However, the direct measurement of $u_s S_s$ of a small-size monopole source is quite challenging. Here, we design a compact detector tube, which combines a balanced armature speaker (Knowles, CI-22955-000) as the sound emitter, a homemade acoustic particle velocity sensor, and a Knowles MEMS silicon microphone, as shown in Fig. 1(a). The detector tube has a width of 6 mm and a height of 10 mm, which are of deep subwavelength scales. The SEM photo of the acoustic particle velocity sensor is shown in Fig. 1(b). The particle velocity sensor consists of three suspended wires above a silicon substrate, and the wires are electrically heated and have a temperature-dependent resistance. The middle wire acts as the heater and the side wires act as temperature sensors. The incident sound wave will induce a temperature difference between the sensing wires, then their resistance difference can be measured, which is proportional to the particle velocity around the wires.

As shown in Fig. 2(a), the detector tube is connected to the structure and the sensors are placed on the contact surface. The acoustic pressure p_s and velocity u_s at the source location are measured, respectively, by the MEMS pressure microphone and the particle velocity sensor. In our setup, S_s becomes the cross-section area of the detector tube. This design gives an excitation-probe setup with a deep subwavelength source and a local detector, which is targeted to probe Green's function in Eq. (4).

In an acoustic cavity such as the Helmholtz resonator [Fig. 2(a)], the resonant LDOS is known to be of the form [32]:

$$\rho(\omega_n) = \frac{2}{\pi \omega_n} \frac{Q}{V}, \quad (6)$$

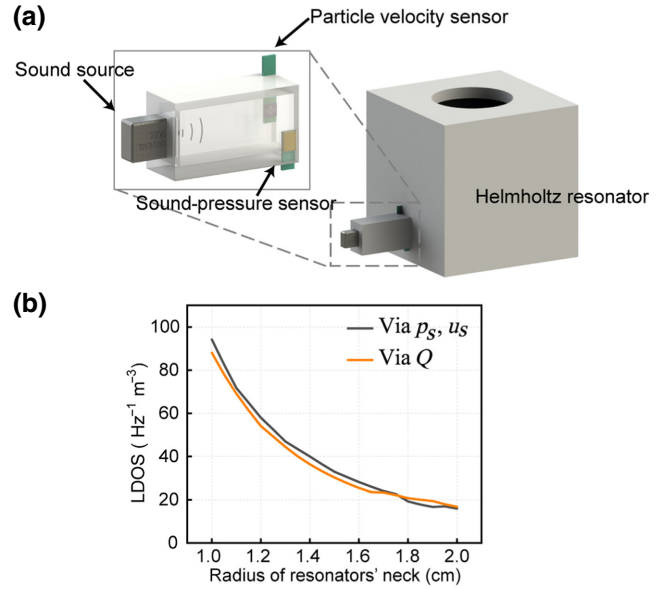


FIG. 2. (a) The detector tube is connected to the testing structure, and can be considered as a subwavelength source. The acoustic pressure and the volume flow rate of source are measured by the sensors. The acoustic LDOS at the source location then can be extracted. (b) The simulation results of acoustic LDOS at the resonance frequency for a Helmholtz resonator with different neck sizes. The results from the quality factor Q of the resonator agree well with the results from the acoustic pressure and velocity at the source location.

where ω_n is the resonance frequency, Q is the quality factor, and V is the modal volume. For the lowest resonant mode, its wave function is nearly homogeneous inside the cavity. The acoustic waves radiate out into the surrounding air through the neck. For a cubic Helmholtz resonator with a side width of 60 mm, we calculate the acoustic LDOS at the resonant frequency for different neck sizes by finite-element simulations. As shown in Fig. 2(b), the results from Eq. (6) agree well with the results from Eq. (5), which demonstrate the feasibility of determining the acoustic LDOS via Eq. (5).

The resonant cavity structures can be utilized to realize the enhancement of LDOS. Here, we measure the acoustic LDOS through setups with two different cavities: the Helmholtz resonator [Fig. 3(a)] and the Fabry-Perot resonator [Fig. 3(c)]. To avoid the subtle influence of residue and environment waves, the experiments are conducted in an anechoic chamber. The speaker is driven by the sound card and the signals of sensors are acquired by the NI 9234 data-acquisition module. As shown in Figs. 3(b) and 3(d), the measured data are in good agreement with the simulation results. The overall LDOS of the Helmholtz resonator is higher than the Fabry-Perot resonator, which is due to the stronger wave confinement in the Helmholtz resonator.

For the acoustic eigenmode, the spatial distribution of LDOS is proportional to the squared acoustic pressure field

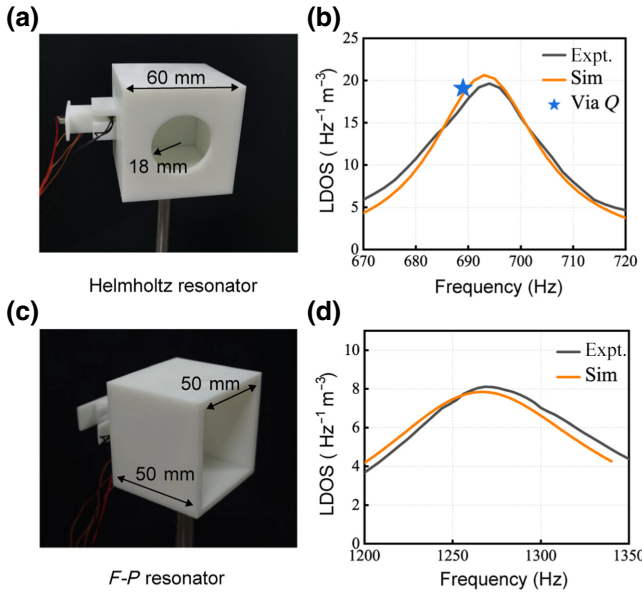


FIG. 3. (a) Photo of the Helmholtz resonator. The detector tube is connected to the resonator and the sensors are placed on the contact surface. (b) The experimental and simulation results of the acoustic LDOS spectrum for the Helmholtz resonator. The blue star corresponds to the resonant LDOS calculated by the quality factor of the resonator. (c) Photo of the Fabry-Perot resonator. The detector tube is placed at the bottom of the resonator, where the LDOS reaches its maximum. (d) The experimental and simulation results of the acoustic LDOS spectrum for the Fabry-Perot resonator.

inside the cavity: $\rho(\omega, \mathbf{r}) \propto |p(\omega, \mathbf{r})|^2$. For the Helmholtz resonator, the LDOS is nearly uniform in the cavity. In contrast, for the Fabry-Perot resonator, the LDOS is inhomogeneous and reaches its maximum at the bottom of the cavity where we probe the LDOS. Figure 4(a) presents the simulated pressure field p distribution of the eigenmode of the Fabry-Perot resonator at 1260 Hz. The pressure field reaches its maximum at the bottom of the cavity. The simulation results of the normalized squared acoustic pressure $|p|^2$ and LDOS $\rho(\mathbf{r})$ at 1260 Hz along the dashed line are shown in Figs. 4(b) and 4(c), respectively, which confirm that $\rho(r) \propto |p(\mathbf{r})|^2$.

IV. ACOUSTIC SSH MODEL AND FRACTIONAL TOPOLOGICAL CHARGE

The LDOS is also tightly connected to the fractional charge in the SSH model and other topological systems. The fractional charge is a signature of the nontrivial topology and can be found in a variety of systems. Here, we use the acoustic SSH model [33–37] as a prototype to measure the fractional topological charge via the LDOS using the above method. The SSH model is a one-dimensional lattice model with staggered hopping amplitudes. By adjusting the intercell and intracell hopping strength, the SSH

model experiences a topological phase transition when band inversion occurs. In its topological phase, the SSH model hosts localized edge states, and the fractional charge emerge at the two ends.

Here, the one-dimensional (1D) acoustic SSH model is realized by coupling an array of acoustic cavities in a dimerized way [Fig. 5(a)]. Each cavity has a height of $L_0 = 150$ mm and a side width of $D_0 = 30$ mm. Two types of square tubes of different widths (5 and 12 mm, respectively) are used to connect the cavities and introduce the dimerized couplings. All tubes are of length 60 mm. The Hamiltonian of the acoustic SSH model, on a real-space basis, is written as

$$H = \begin{bmatrix} E_0 & v & 0 & \cdots & 0 \\ V & E_0 & w & \cdots & \vdots \\ 0 & w & E_0 & \cdots & 0 \\ \vdots & \vdots & \vdots & \ddots & v \\ 0 & \cdots & 0 & v & E_0 \end{bmatrix}, \quad (7)$$

where E_0 denotes the on-site potential, and v (w) is the intracell (intercell) hopping, which is related to the width of the coupling tube. The LDOS of the acoustic SSH model can be theoretically calculated from the real-space Hamiltonian (see Appendix A for details). When the intracell coupling is stronger (weaker) than the intercell coupling, the system is trivial (topological). Figures 5(b) and 5(c) show the acoustic eigenstate spectrum from finite-element simulations for the topological and trivial cases. There are in total 16 eigenstates in the spectrum for both cases, which is equal to the number of cavities in our system. For the topological case, there are two edge states emerging at the middle of the band gap. Figures 5(d) and 5(e) show the pressure-field distributions of the edge state [Fig. 5(d)] and the bulk state [Fig. 5(e)] of the 1D acoustic SSH model from finite-element simulations. The edge state is mainly localized in the edge cavity, while the bulk state occupies the other cavities.

The sample is fabricated using three-dimensional (3D) printing technology [Fig. 6(a)] and has eight unit cells. There are two sites within each unit cell. In the experiment, the detector tubes are placed at the top of the cavities. We measure the LDOS of each cavity with a frequency step of 2 Hz. We define that the LDOS at the i th site is $\rho(f, i) = (1/2)\rho_{\max}(f, i)L_0D_0^2$ where $\rho_{\max}(f, i)$ is the maximum LDOS in the i th cavity (i.e., the LDOS measured at the top of the cavity, see Appendix B for details). In Fig. 6(b), we present the LDOS $\rho(f, i)$ for the first four sites of the system using results from theoretical calculations, finite-element simulations, and the experimental data for the topological case. These results are in agreement with each other. We find that for the LDOS in site 1, the edge state emerges as a single peak in the band gap. For the LDOS in sites 2–4, the two peaks are associated with the

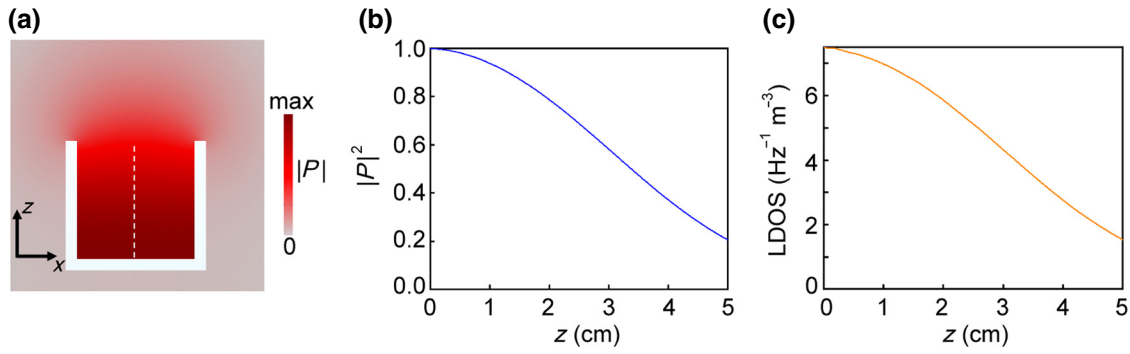


FIG. 4. (a) Simulated pressure-field p distribution of the eigenmode of the Fabry-Perot resonator at 1260 Hz. (b),(c) The simulation results of the normalized $|p|^2$ and LDOS $\rho(\mathbf{r})$ along the white dashed line, which confirm that the spatial distribution of LDOS is proportional to the squared acoustic pressure field inside the cavity.

bulk states. From these results, we can infer that the edge states are mainly localized in the edge cavities, which is in agreement with the simulated pressure-field distribution of the edge state in Fig. 5(d).

In its topological phase, the SSH model supports the fractional charge at edges. The topology of the SSH model can be characterized by the bulk polarization as $P = (i/2\pi) \int dk \langle u(k) | \partial_k u(k) \rangle$, which is the integral of the Berry potential over the Brillouin zone, with $u(k)$ being the Bloch function. $P = 0(1/2)$ corresponds to the trivial (topological) case. The Wannier center, which indicates the charge distribution, is identical to the bulk polarization. The position of the Wannier centers is shown in Fig. 6(c). The Wannier centers are at the center (edge) of the unit cell in the trivial (topological) case. Thus, in the topological case, the Wannier center is shared by two adjacent unit cells and contribute $1/2$ charge to each of them, which indicates a nontrivial phase with fractional edge charge.

The fractional charge can be understood via the concept of filling anomaly [38,39]: the mismatch between the number of valence-band eigenstates to the number of unit cells and the inversion symmetry leads to the fractional charge of $1/2$.

In analog of the fermionic band filling of the valence band and the edge states, here the mode charge for each site is defined as

$$q_i = \int_0^{f_{\text{gap}}} \rho(f, i) df. \quad (8)$$

Here, f_{gap} is a frequency in the band gap and is above the edge states. The mode charge of each unit cell is the sum of the mode charge of the two sites. The results are shown in Fig. 6(c). For the trivial case, the mode charge of each unit cell is close to the theoretical value of 1. For the topological case, it is shown that the edge unit cell has a mode charge

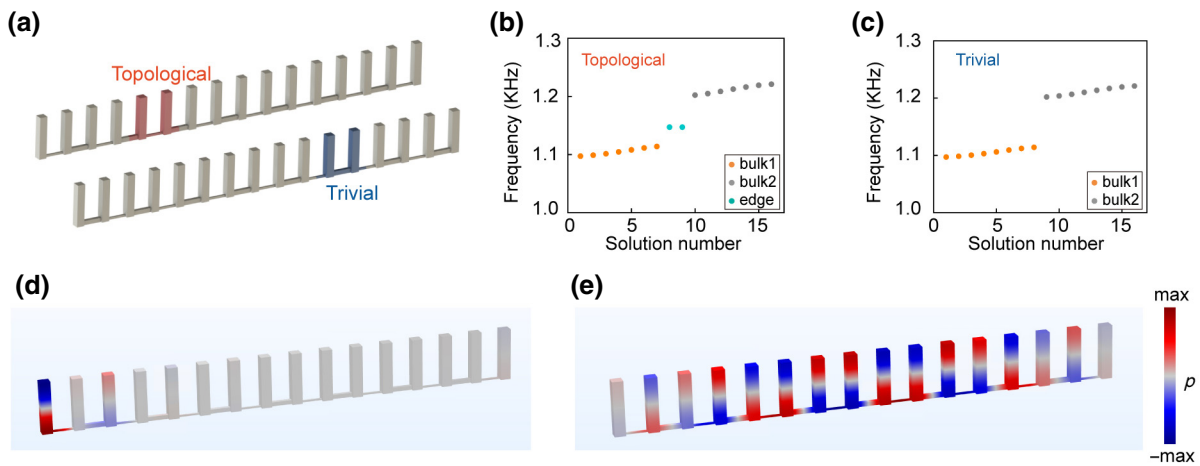


FIG. 5. (a) The structure of the 1D acoustic SSH model. The eigenstate spectrum from finite-element simulations for the topological (b) and trivial case (c). A pair of edge states emerge in the band gap for the topological case. Here, “bulk 1” and “bulk 2” label the valence and conduction bands, respectively. (d),(e) Simulation results of the field distributions of the edge state (d) and bulk state (e) of the acoustic SSH model.

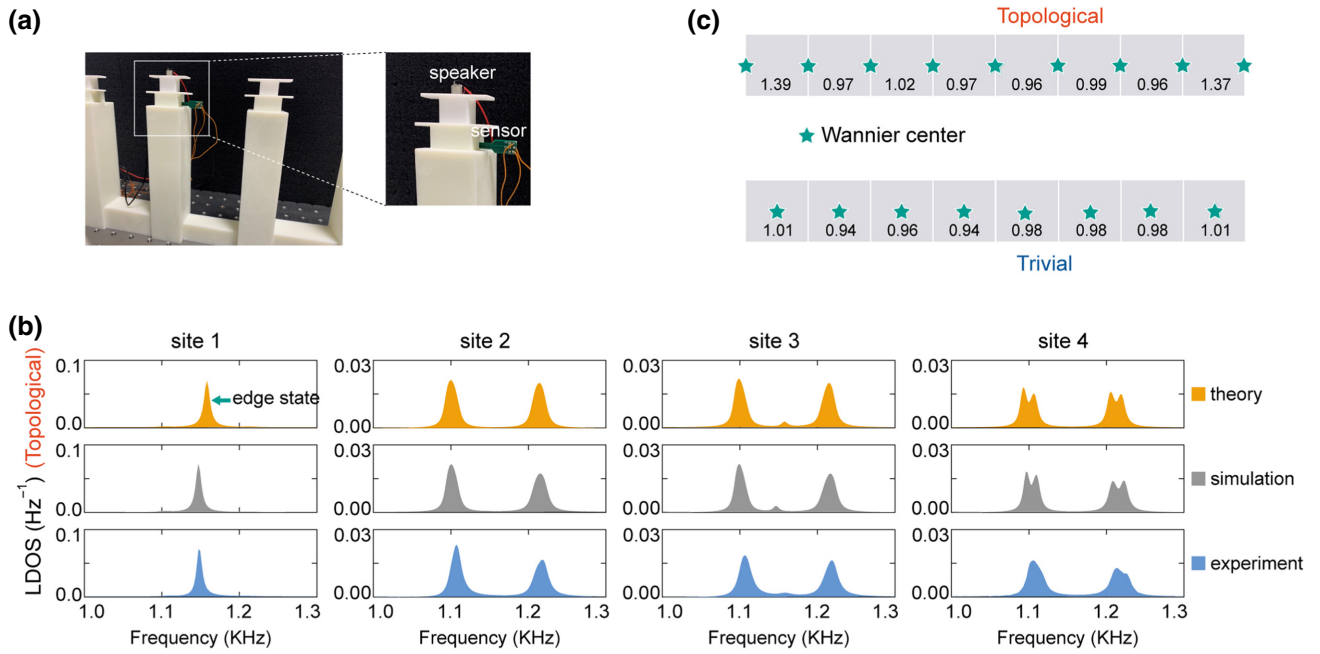


FIG. 6. (a) Photo of the sample. Inset shows the structure of the device for the probe of the acoustic LDOS. (b) The LDOS spectrum of the first four sites of the system. In the LDOS spectrum of site 1, the edge state emerges as a single peak in the band gap. In the LDOS spectrum of sites 2–4, the two peaks correspond to the bulk states. (c) Measured mode charge of each unit cell for the topological and trivial case. The green stars label the Wannier centers.

close to 1.5, which reveals the $1/2$ fractional topological charge for the SSH model.

V. CONCLUSIONS

In this work, we develop a method to probe the acoustic LDOS through the measurement of the volume flow rate and the acoustic pressure with a local excitation-probe configuration. In acoustic systems, the characterization of the acoustic field is usually based on measurement of the sound pressure, which ignores the particle velocity. Here, we characterize the properties of the subwavelength acoustic source via the combination of an acoustic particle velocity sensor and a pressure microphone, and the acoustic LDOS at the source location then can be directly extracted. Based on this method, we observe in an acoustic SSH system the emergence of $1/2$ fractional topological charge, which proves that our method can help identify the band topology of topological acoustic phases. These findings reveal the central relevance of the LDOS in acoustic systems and thus opens a pathway toward the fundamental physics of acoustic phenomena [30,40]. The measurement of acoustic LDOS could also have many practical applications. The low-frequency acoustic emission enhancement is highly demanded in audio acoustics. The engineering of LDOS via acoustic structures can control and enhance the emission rate of acoustic sources. Calculating and measuring the LDOS is therefore necessary for the spatial and spectral control of acoustic emissions. The tailoring of

LDOS can also play a role in acoustic wave-matter interaction, energy confinement [41], and sound absorption. Moreover, the measurement of LDOS provides a useful tool for the characterization of acoustic systems, such as probing the band structure and eigenmodes of phononic crystals [42].

ACKNOWLEDGMENTS

The work is jointly supported by the National Key R&D Program of China (Grants No. 2021YFB3801801, No. 2017YFA0303702, No. 2017YFA0305100, and No. 2018YFA0306200), the National Natural Science Foundation of China (Grants No. 52203358, No. 11890702, No. 12125504, No. 51721001, and No. 12074281). We also acknowledge the support of the Natural Science Foundation of Jiangsu Province, Jiangsu specially appointed professor funding, and the support from the Priority Academic Program Development of Jiangsu Higher Education Institutions (PAPD).

APPENDIX A: CALCULATING LDOS FROM THE REAL-SPACE HAMILTONIAN

In quantum mechanics, Green's function of the Hamiltonian is a useful concept, which closely links to the density of states. Green's function can be obtained by the

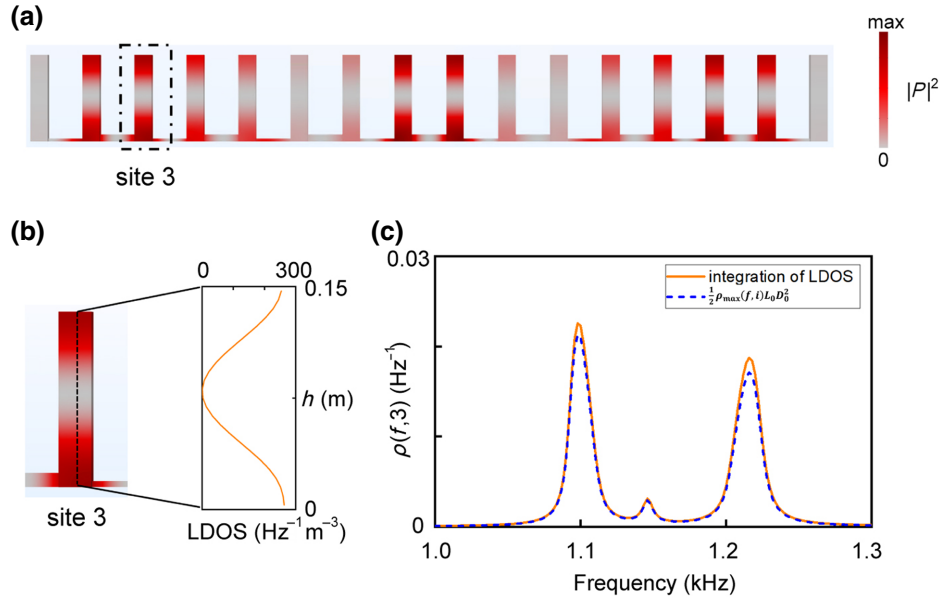


FIG. 7. (a) Simulation results of the squared pressure $|p|^2$ distribution of the eigenmode at 1216 Hz. (b) Simulation results of the LDOS distribution inside the third cavity at 1216 Hz. (c) Simulation results of the LDOS spectrum of the third site. The results from $(1/2)\rho_{\max}(f, i)L_0D_0^2$ agree well with the results by integrating the LDOS over the whole site. $\rho_{\max}(f)$ is the maximum LDOS on top of the third cavity.

real-space Hamiltonian via

$$G^\pm(E, \mathbf{r}, \mathbf{r}') = \frac{1}{E \pm i\eta - H}. \quad (\text{A1})$$

It can also be expressed by the eigenfunctions:

$$G^\pm(E, \mathbf{r}, \mathbf{r}') = \sum_n \frac{\varphi_n(\mathbf{r})\varphi_n^*(\mathbf{r}')}{E \pm i\eta - \lambda_n}. \quad (\text{A2})$$

Using $\lim_{\eta \rightarrow 0^+} (1/x \pm i\eta) = P(1/x) \mp i\pi\delta(x)$:

$$G^\pm(E, \mathbf{r}, \mathbf{r}') = P \sum_n \frac{\varphi_n(\mathbf{r})\varphi_n^*(\mathbf{r}')}{E - \lambda_n} \mp i\pi \sum_n \delta(E - \lambda_n)\varphi_n(\mathbf{r})\varphi_n^*(\mathbf{r}'). \quad (\text{A3})$$

The LDOS is defined as

$$\rho(\mathbf{r}, E) = \sum_n \delta(E - \lambda_n)\varphi_n(\mathbf{r})\varphi_n^*(\mathbf{r}). \quad (\text{A4})$$

Comparing Eqs. (A3) and (A4), we can find that the LDOS corresponds to the imaginary part of Green's function:

$$\rho(\mathbf{r}, E) = \mp \frac{1}{\pi} \text{Im}G^\pm(E, \mathbf{r}, \mathbf{r}) \quad (\text{A5})$$

and the DOS is the trace of the matrix:

$$\rho(E) = \mp \frac{1}{\pi} \text{Im}[\text{tr}G^\pm(E)]. \quad (\text{A6})$$

APPENDIX B: DISTRIBUTION OF LDOS INSIDE THE ACOUSTIC SSH MODEL

In Fig. 7(a), we present the calculated squared pressure $|p|^2$ distribution of the eigenmode at 1216 Hz, which is proportional to the LDOS. The calculated LDOS distribution inside the cavity at 1216 Hz is shown in Fig. 7(b). The acoustic pressure of the cavity mode is described by a sinusoidal function along the z direction. As a result, the average acoustic LDOS inside the cavity is equal to $(1/2)\rho_{\max}(f)$, where $\rho_{\max}(f)$ is the maximum LDOS at the top of the cavity. The LDOS inside the coupling tube is difficult to be measured, and can be ignored because the size of the tube is much smaller than the cavity. The LDOS at the i th site is then given by $\rho(f, i) = (1/2)\rho_{\max}(f, i)L_0D_0^2$. In Fig. 7(c), we present the LDOS spectrum of the third site by finite-element simulations. The results from $(1/2)\rho_{\max}(f, i)L_0D_0^2$ agree well with the results by integrating the LDOS over the whole site. The results from $(1/2)\rho_{\max}(f, i)L_0D_0^2$ are smaller than the results from integration because we ignore the LDOS inside the tube.

[1] E. M. Purcell, Spontaneous emission probabilities at radio frequencies, *Phys. Rev.* **69**, 681 (1946).

[2] J. M. Gérard, B. Sermage, B. Gayral, B. Legrand, E. Costard, and V. Thierry-Mieg, Enhanced Spontaneous Emission by Quantum Boxes in a Monolithic Optical Microcavity, *Phys. Rev. Lett.* **81**, 1110 (1998).

- [3] S. Noda, M. Fujita, and T. Asano, Spontaneous-emission control by photonic crystals and nanocavities, *Nat. Photonics* **1**, 449 (2007).
- [4] E. Yablonovitch, Inhibited Spontaneous Emission in Solid-State Physics and Electronics, *Phys. Rev. Lett.* **58**, 2059 (1987).
- [5] P. Lodahl, A. F. v. Driel, I. S. Nikolaev, A. Imman, K. Overgaag, D. I. Vanmaekelbergh, and W. L. Vos, Controlling the dynamics of spontaneous emission from quantum dots by photonic crystals, *Nature* **430**, 654 (2004).
- [6] A. N. Poddubny, P. A. Belov, and Y. S. Kivshar, Purcell effect in wire metamaterials, *Phys. Rev. B* **87**, 035136 (2013).
- [7] R. Carminati, A. Cazé, D. Cao, F. Peragut, V. Krachmalnicoff, R. Pierrat, and Y. De Wilde, Electromagnetic density of states in complex plasmonic systems, *Surface Sci. Rep.* **70**, 1 (2015).
- [8] A. Poddubny, I. Iorsh, P. Belov, and Y. Kivshar, Hyperbolic metamaterials, *Nat. Photonics* **7**, 948 (2013).
- [9] Z. Jacob, I. I. Smolyaninov, and E. E. Narimanov, Broadband Purcell effect: Radiative decay engineering with metamaterials, *Appl. Phys. Lett.* **100**, 181105 (2012).
- [10] M. A. Noginov, Y. A. B. H. Li, G. N. D. Dryden, C. E. B. G. Zhu, Z. J. M. Mayy, and E. E. Narimanov, Controlling spontaneous emission with metamaterials, *Opt. Lett.* **35**, 1863 (2010).
- [11] K. Song, S. H. Lee, K. Kim, S. Hur, and J. Kim, Emission enhancement of sound emitters using an acoustic metamaterial cavity, *Sci. Rep.* **4**, 4165 (2014).
- [12] J. Zhao, L. Zhang, and Y. Wu, Enhancing monochromatic multipole emission by a subwavelength enclosure of degenerate Mie resonances, *J. Acoust. Soc. Am.* **142**, EL24 (2017).
- [13] X.-D. Fan, Y.-F. Zhu, B. Liang, J.-c. Cheng, and L. Zhang, Converting a Monopole Emission into a Dipole Using a Subwavelength Structure, *Phys. Rev. Appl.* **9**, 034035 (2018).
- [14] F. Liu, W. Li, and M. Ke, Rigorous Analytical Model for Multipole Emission Enhancement Using Acoustic Metamaterials, *Phys. Rev. Appl.* **10**, 054031 (2018).
- [15] M. Landi, J. Zhao, W. E. Prather, Y. Wu, and L. Zhang, Acoustic Purcell Effect for Enhanced Emission, *Phys. Rev. Lett.* **120**, 114301 (2018).
- [16] L. Langguth, R. Fleury, A. Alu, and A. F. Koenderink, Drexhage's Experiment for Sound, *Phys. Rev. Lett.* **116**, 224301 (2016).
- [17] M. K. Schmidt, L. G. Helt, C. G. Poulton, and M. J. Steel, Elastic Purcell Effect, *Phys. Rev. Lett.* **121**, 064301 (2018).
- [18] Ø Fischer, M. Kugler, I. Maggio-Aprile, C. Berthod, and C. Renner, Scanning tunneling spectroscopy of high-temperature superconductors, *Rev. Mod. Phys.* **79**, 353 (2007).
- [19] M. D. Birowosuto, S. E. Skipetrov, W. L. Vos, and A. P. Mosk, Observation of Spatial Fluctuations of the Local Density of States in Random Photonic Media, *Phys. Rev. Lett.* **105**, 013904 (2010).
- [20] C. W. Peterson, T. Li, W. A. Benalcazar, T. L. Hughes, and G. Bahl, A fractional corner anomaly reveals higher-order topology, *Science* **368**, 1114 (2020).
- [21] Y. Liu, S. Leung, F. F. Li, Z. K. Lin, X. Tao, Y. Poo, and J. H. Jiang, Bulk-disclination correspondence in topological crystalline insulators, *Nature* **589**, 381 (2021).
- [22] C. W. Peterson, T. Li, W. Jiang, T. L. Hughes, and G. Bahl, Trapped fractional charges at bulk defects in topological insulators, *Nature* **589**, 376 (2021).
- [23] B. Xie, R. Huang, S. Jia, Z. Lin, J. Hu, Y. Jiang, S. Ma, P. Zhan, M. Lu, Z. Wang, Y. Chen, and S. Zhang, Bulk-LDOS correspondence in topological insulators, *arXiv:2209.02347* (2022).
- [24] V. Peri, Z.-D. Song, M. Serra-Garcia, P. Engeler, R. Queiroz, X. Huang, W. Deng, Z. Liu, B. A. Bernevig, and S. D. Huber, Experimental characterization of fragile topology in an acoustic metamaterial, *Science* **367**, 797 (2020).
- [25] M. Miniaci, F. Allein, and R. K. Pal, Spectral flow of a localized mode in elastic media, *arXiv:2111.09021* (2021).
- [26] R.-J. Slager, A. Mesaros, V. Juričić, and J. Zaanen, Interplay between electronic topology and crystal symmetry: Dislocation-line modes in topological band insulators, *Phys. Rev. B* **90**, 241403 (2014).
- [27] J. C. Y. Teo and C. L. Kane, Topological defects and gapless modes in insulators and superconductors, *Phys. Rev. B* **82**, 115120 (2010).
- [28] R.-J. Slager, The translational side of topological band insulators, *J. Phys. Chem. Solids* **128**, 24 (2019).
- [29] Y. Ran, Y. Zhang, and A. Vishwanath, One-dimensional topologically protected modes in topological insulators with lattice dislocations, *Nat. Phys.* **5**, 298 (2009).
- [30] B. Xie, H.-X. Wang, X. Zhang, P. Zhan, J.-H. Jiang, M. Lu, and Y. Chen, Higher-order band topology, *Nat. Rev. Phys.* **3**, 520 (2021).
- [31] P. Sheng, *Introduction to wave scattering, localization, and mesoscopic phenomena* (Springer, New York, 2006).
- [32] A. Oskooi and S. G. Johnson, Electromagnetic wave source conditions, *arXiv:1301.5366* (2013).
- [33] M. Xiao, G. Ma, Z. Yang, P. Sheng, Z. Q. Zhang, and C. T. Chan, Geometric phase and band inversion in periodic acoustic systems, *Nat. Phys.* **11**, 240 (2015).
- [34] X. Li, Y. Meng, X. Wu, S. Yan, Y. Huang, S. Wang, and W. Wen, Su-Schrieffer-Heeger model inspired acoustic interface states and edge states, *Appl. Phys. Lett.* **113**, 203501 (2018).
- [35] A. Coutant, A. Sivadon, L. Zheng, V. Achilleos, O. Richoux, G. Theoharis, and V. Pagneux, Acoustic Su-Schrieffer-Heeger lattice: Direct mapping of acoustic waveguides to the Su-Schrieffer-Heeger model, *Phys. Rev. B* **103**, 224309 (2021).
- [36] L.-Y. Zheng, V. Achilleos, O. Richoux, G. Theoharis, and V. Pagneux, Observation of Edge Waves in a Two-Dimensional Su-Schrieffer-Heeger Acoustic Network, *Phys. Rev. Appl.* **12**, 034014 (2019).
- [37] Z.-G. Chen, L. Wang, G. Zhang, and G. Ma, Chiral Symmetry Breaking of Tight-Binding Models in Coupled Acoustic-Cavity Systems, *Phys. Rev. Appl.* **14**, 024023 (2020).
- [38] W. A. Benalcazar, T. Li, and T. L. Hughes, Quantization of fractional corner charge in Cn-symmetric higher-order topological crystalline insulators, *Phys. Rev. B* **99**, 245151 (2019).

- [39] C. Liang, Y. Liu, F.-F. Li, S. Leung, Y. Poo, and J.-H. Jiang, Observation of fractional topological numbers at photonic edges and corners, [arXiv:2203.00206](#) (2022).
- [40] G. Ma, M. Xiao, and C. T. Chan, Topological phases in acoustic and mechanical systems, *Nat. Rev. Phys.* **1**, 281 (2019).
- [41] S. Huang, S. Xie, H. Gao, T. Hao, S. Zhang, T. Liu, Y. Li, and J. Zhu, Acoustic Purcell effect induced by quasibound state in the continuum, *Fundam. Res.* (2022).
- [42] R. Sapienza, T. Coenen, J. Renger, M. Kuttge, N. F. van Hulst, and A. Polman, Deep-subwavelength imaging of the modal dispersion of light, *Nat. Mater.* **11**, 781 (2012).